

Composite Ship Track Characteristics

P. A. DURKEE¹, R. E. CHARTIER¹, A. BROWN¹, E. J. TREHUBENKO¹,
S. D. ROGERSON¹, C. SKUPNIEWICZ¹, K. E. NIELSEN¹, S. PLATNICK² AND M. D. KING²

¹*Naval Postgraduate School, Monterey, California*

²*NASA Goddard Space Flight Center, Greenbelt, Maryland*

Corresponding Author: Philip A. Durkee, Naval Postgraduate School, 589 Dyer Road,
Monterey, CA, 93943-5113, Email: durkee@nps.navy.mil

ABSTRACT

The physical and radiative properties of a composite ship track are described from the analysis of 131 ship/ship track correlation pairs collected during the Monterey Area Ship Track (MAST) Experiment. The significant variability of ship tracks around their average characteristics is also described. The nominal environmental conditions for the ship track set are also described. The composite ship track is $296(\pm 233)$ standard deviation km long, $7.3(\pm 6)$ hours old, and averages $9(\pm 5)$ km wide. The ship is, on the average $16(\pm 8)$ km from the head of the ship track along the relative wind vector and corresponds to a time of $25(\pm 15)$ minutes. The set of ship tracks examined in this study formed in marine boundary layers that were between 300 and 750 m deep, and no tracks formed in boundary layers above 800 m. The tracks form in high relative humidity, small air-sea temperature differences, and moderate winds (average of $7.7(\pm 3.1)$ m s⁻¹). The ambient cloud reflectance in AVHRR channel 3 (3.7 μ m wavelength) is $11(\pm 4)\%$ while the composite ship track value is $14(\pm 5)\%$. The relative track brightness is $7(\pm 26)\%$ and $37(\pm 34)\%$ for 0.63 μ m and 3.7 μ m wavelengths respectively.

1. Introduction

As early as 1944 mariners reported cloud formations and alterations of existing clouds over the exhaust plume of ships. For over thirty years the effects of ships on clouds have been observed in visible satellite imagery (Conover, 1966). More recently, Coakley et al. (1987) described ship effects on clouds in near-infrared imagery. These perturbations of the marine cloud field, called ship tracks, are narrow, curvilinear regions of enhanced cloud reflectance. In 1994, the Monterey Area Ship Track (MAST) Experiment was conducted to answer fundamental questions of ship track formation (Durkee et al., this issue). MAST was designed to test a series of formation hypotheses that centered on links between the aerosol generated in the ships stack, mixing of the effluent through the cloud-topped marine boundary layer, and subsequent reduction in cloud droplet size. The definition of a ship track adopted by the MAST science team is taken from its near-infrared signature - a curvilinear, bright feature in near-infrared imagery that is spatially coincident with the effluent plume of a ship.

In order to address questions about ship track formation mechanisms, necessary environmental conditions, and their long persistence, we must understand the environment in which they form and their resultant physical and radiative characteristics. Not every ship causes a ship track and ship tracks are seldom observed in some geographical locations, while they are prevalent in others. A combination of ambient conditions is apparently necessary in the marine atmosphere before a given ship can produce a ship track. Conover (1966) and Bowley (1967) suggested several conditions from early observations from TIROS satellites. The conditions suggested were; (1) a shallow, cloud-topped, well-mixed boundary layer, (2) a low number of cloud condensation nuclei (CCN), and (3) a relatively narrow range of temperature and relative humidity values at the surface. Although MAST was not designed to test all of the possible conditions necessary for ship track formation, this paper presents analysis of the influence of boundary layer depth on ship track formation.

A more complete knowledge of ship track characteristics will help quantify the process by which anthropogenic aerosols increase cloud reflectance, decrease solar heating and force local and global climate response (Albrecht, 1989; Charlson et al., 1987; Charlson et al., 1992). This paper presents a composite analysis of ship track properties. Satellite imagery from 131 ship tracks produced by known ships provides the basis to: (1) describe and quantify nominal

ship track physical and radiative characteristics, (2) determine if ship specific characteristics such as, propulsion type or power rating, influence ship track radiative properties, and (3) test relevant MAST hypotheses through the use of composite ship track characteristics and statistics (see Durkee et al. this issue).

2. Ship track formation and background environmental conditions

a. Marine boundary layer depth

Two data sets are available to test the significance of boundary layer depth on the potential for ship track formation. First, in July 1991, SEAHUNT (Ship-trail Evolution Above High Updraft Naval Targets) was conducted off the southern California and Baja Mexico coasts (Porch et al., 1995). The R/V *Egabrag* hosted measurements of aerosol, CCN, radiation and meteorological measurements including balloon soundings. An average of two radiosondes at 1200 and 2400 UTC daily were collected during SEAHUNT. This data was used to analyze boundary layer depth above the R/V *Egabrag*. Surface observations of sea-surface temperature (SST) and cloud conditions were also used in the analysis described here.

Second, in June 1994, the Monterey Area Ship Track (MAST) Experiment was conducted off the central California coast (Durkee et al., this issue). Aboard the R/V *Glorita*, radiosondes were launched six times daily at four-hour intervals. Surface measurements of SST and meteorological conditions from the *Glorita* were also used in this study.

A total of 33 radiosondes from SEAHUNT and 94 soundings from MAST are used here and compared to ship track formation frequency. NOAA Advanced Very High Resolution Radiometer (AVHRR) 3.7 μm wavelength images of stratus cloud were compared to soundings considered to be representative of the ship track environment. Soundings that were collected within three hours of the satellite overpass were taken as representative of the environment at the time of the ship track formation. The *Egabrag* and *Glorita* ships were considered to be in a ship track conducive region if tracks were found within 300 km and the thermal cloud characteristics determined from the 11 μm wavelength image were homogeneous. Homogeneity was satisfied if the cloud-top temperature was within 0.5 C of the cloud over the sounding position. The image was also examined for sharp gradients in cloud texture. Ship tracks located across a cloud-texture boundary were not included in the analysis of track formation regions.

An important assumption in this study is a constant distribution of shipping in the SEAHUNT and MAST regions. Observations of imagery during MAST (Durkee et al., this issue; Coakley et al., this issue) show that ship tracks occur in groups, and single tracks within large, cloud-covered regions are rare. When conditions are not conducive to track development, there is a noticeable lack of ship tracks over very large regions. This implies that, on the average, when cloud is present in the image but no ship tracks are detected, environmental factors are the cause of the lack of tracks and not gaps in shipping.

Figure 1 shows a histogram over boundary layer height of conducive and non-conductive cases from the analysis of the SEAHUNT and MAST data sets. The distribution for both experiments clearly shows a reduction in ship track occurrence for greater boundary layer height. In fact, no track-conductive cases were found with boundary layer height greater than about 750 m.

Combining the data sets from MAST and SEAHUNT provides a broader context for a statistical analysis of ship track occurrence in the Californian stratus region. The SEAHUNT data set has deeper boundary layers, on average, than the MAST data set. This is due to the climatologically expected increase in boundary layer depth under the southern side of the subtropical high pressure system. Figure 1 shows that even though SEAHUNT boundary layer depths are greater than for MAST, both data sets show a sharp decrease in track occurrence around 700 m.

The solid line in Figure 1 shows the average number of tracks per case as a function of boundary layer height. It is clear that track number also varies strongly with boundary layer height. For the cases analyzed in this study, the most tracks form for boundary layer height of 450 m and track number quickly falls to zero above about 700 m. This is corroborated by Coakley et al. (this issue) who shows ship track formation decreasing rapidly as boundary layer depth increases above 800-1000 m altitude.

The drop-off of track occurrence with increasing boundary layer depth is consistent with lower concentrations of the ship-generated aerosol, and therefore CCN, in deeper boundary layers. A ship would need to produce twice the CCN concentration in a 700 m deep boundary layer than in a 350 m deep boundary layer to cause the same increase in CCN at the base of the cloud. Reduced concentration of CCN at cloud base results in a reduced forcing on the microphysical properties of the cloud and thereby a weaker radiative signature. In addition,

deeper boundary layers are more likely to have internal stable layers that inhibit mixing of the surface layer constituents, including ship effluent, throughout the marine boundary layer (Bretherton et al., this issue). Figure 1 also shows some evidence of a decrease in track frequency for boundary layers below 400 m depth. However, the number of cases at these low boundary layer depths is very small in the available data set and very little confidence can be attached to this observation.

b. The Composite Ship track Environment

During MAST and SEAHUNT the research ships also made surface meteorological measurements. Table 1 contains mean, maximum, and minimum values and standard deviations of environmental parameters for ship track and non-ship track conditions. Both track and non-track conditions are characterized by high relative humidity, small air-sea temperature differences, and moderate winds in a shallow cloud-topped marine atmospheric boundary layer. As discussed above, the greatest difference in Table 1 is boundary layer depth showing that ship tracks occurred in shallower boundary layers than for non-ship track conditions (see also Coakley et al., this issue).

3. Composite analysis of ship track characteristics

a. Procedures

Ship tracks and ship track heads were visually identified, and cataloged from NOAA 9/10/11/12 AVHRR satellite imagery collected during the MAST experiment. Up to 10 passes per day were obtained from these polar orbiting platforms and the greatest gap in coverage was between four to six hours. Figure 2 shows the geographical locations of the 1362 ship track heads identified during the month of the experiment. As might be expected, a heavy concentration of head points lie along the great-circle shipping lanes.

Accurate ship position data were used to make correlations between ship tracks and the ship that formed it. The ship position data were acquired from three sources. Fleet Numerical Meteorology and Oceanography Center (FNMOC) provided positions of ships on the ship synoptic weather reporting system. The ships report their international call sign, position, various weather parameters including the true wind and the date-time-group. The bulk of the reports are at synoptic weather reporting times (0000, 0600, 1200, 1800 UTC). These reports provided 7693 ship and buoy positions during the MAST experiment.

The second source was the Joint Maritime Information Element (JMIE) Support System (JSS). It provided 10,788 ship position reports. The JSS is a U.S. Coast Guard (USCG) maintained database and consists of multi-source, world-wide, maritime-related data, pooled into one central database. These data included off-synoptic time reports as well as most of the FNMOC reports. Thus, many of the gaps in the FNMOC data were filled by JSS data.

MAST research aircraft also provided some ship position reports, albeit limited in number. Some of these reports were essential to make correlations near land where ships are less likely to report due to navigational and operational considerations.

1) Correlations

A correlation consists of an identified ship track and the name and position of the ship that formed it. For a correlation to be made the ship and the ship track must be collocated in space and at the same time. In addition, the youngest portion of the ship track must be oriented in the direction of the relative wind for that ship. The oldest portion of the ship track must also display an appearance in agreement with the true wind field pattern. That is, a westbound ship with northerly winds has a relative wind from the northwest and a ship track that extends southeast of the ships position.

The ship characteristic data was derived from four primary sources:

1. Lloyd's Register of Shipping 1992-1993.
2. The USCG Marine Safety Information System (MSIS).
3. The Office of Naval Intelligence Merchant Ship Characteristics (MSC).
4. The USCG JSS.

The sources that provided the most data are listed first. MSIS and JSS data is available by on line computer queries. The other two sources are in hard copy form. No one source contained all the information. However, Lloyd's Register was by far the most complete.

The set of correlations used for this study was limited by daytime only cases so that of 209 correlations from the MAST data set, only 131 correlations are presented here in the composite analysis. The information gathered for each of the 209 correlations included:

1. gross tonnage
2. propulsion type - steam or diesel

3. fuel type
4. power rating (kW)
5. length (m)
6. course and speed
7. true wind (observed)
8. relative wind (calculated)

Table 2 lists a summary of correlations by propulsion type. The value in parenthesis is the number used for this study.

2) Retrieval of ship track characteristics

The retrieval of physical and radiative characteristics is done through an automated process using all five channels of the AVHRR:

1. 0.58-0.68 μm wavelength
2. 0.68-1.1 μm wavelength
3. 3.5-3.9 μm wavelength
4. 10.3-11.3 μm wavelength
5. 11.3-12.3 μm wavelength

To get cloud reflectance, an anisotropic reflectance factor (ARF, the ratio of the hemispheric reflectance to directional reflectance) is used to correct for the specific angular geometry between sun, reflecting surface, and satellite for each pixel (Mineart, 1988 and Brenner, 1994). AVHRR products generated for this study were LOW1 (low cloud reflectance; channel 1 ARF applied), LOW3 (low cloud reflectance; channel 3 ARF applied), and CTT4 (cloud top temperature; channel 4).

The extraction process evaluates the radiative signature of the ship track and the surrounding ambient cloud. This analysis is done for each kilometer distance down the track. The algorithm creates a remapped 61 km swath along the track by interpolation onto a one kilometer, equal area grid. The center of the swath is determined by the highest LOW3. The

track edge is defined by the largest LOW3 reflectance gradient on each side of the bright center. At one kilometer beyond this gradient, on both sides of the centerline, five pixels are used to calculate an average ambient LOW1, LOW3 and CTT4 for that 1 km length of track. The data are discarded if the standard deviation of the five ambient CTT4 values is greater than 0.5 C to remove partly cloudy portions of the track from the composite statistics.

b. Composite spatial characteristics

1) Ship-ship track separation distance

Ship tracks begin to appear in satellite imagery when the ship plume has widened sufficiently to brighten a single image element (pixel) - 1.1 km at nadir in the case of AVHRR. This first bright feature or ship track head is therefore some distance from the ship determined by the time required for the ship plume to broaden by turbulent dispersion processes. Figure 3 shows ship effects on a smaller scale than in AVHRR imagery. The image was taken by shuttle astronauts during mission STS-65 off the western coast of Chile on 20 July 1994. The resolution of the image (30 m) in this case is less than the size of cloud elements created within the ship plume (Kirschbaum, 1994). The width of the first cloud feature at the head of the ship track is 130 m. The cloud features reach 1 km width at about 10 km downtrack from the head. This means, by extrapolation, that the ship would be about 11 km from the head if this ship track were observed in AVHRR imagery.

The ER-2 aircraft operated an RC-10 high resolution, broadband (0.51 to 0.90 μm wavelength) camera system during MAST. Figure 4 is an image from the RC-10 at 1840 UTC on 13 June 1994 and shows a cargo ship and the early formation of a ship track. In this case the ship is moving in the direction of, but slower than, the wind and the ship track therefore extends out ahead of the ship. The enlarged region of Figure 4 shows the ship and white-capped waves near the bow and in the wake behind the ship. The first bright cloud down the relative wind vector is about 5.5 ship lengths from the ships stack (located in the stern). Examination of the MODIS Airborne Simulator images (also flown on the ER-2) indicates the cargo ship length is about 250 m. Using the ship length as a reference, the distance to the first perturbed cloud is about 1400 m. The first cloud that is noticeably brighter than the background is about 50 m across. The first bright cloud element large enough to fill half of a 1.1 km AVHRR field-of-view is 5 km from the ship stack.

The MRF C-130 observed cloud-top heights to be about 400 m throughout the day in the vicinity of the ship in Figure 4. The MAST ship R/V *Glorita* observed wind speeds of 10-12 m s⁻¹. If the cargo ship is assumed to move 1 m s⁻¹ slower than the true wind, the time required for the ship effluent to move downtrack to the distance of the first bright cloud will be about 1400 s. This suggests the boundary layer turbulence must mix the effluent through the 400 m boundary layer and enhance the cloud formation process within 23 minutes of release from the ship.

The ship-to-ship track separation data from the 99 best correlations were calculated using interpolation of ship reported positions to image times. Figure 5 is a plot of the calculated ship position for the 99 correlations relative to the ship track head observed in AVHRR data. If there were no errors in the calculation of ship position, all the points would fall on the zero-degree line with distance determined by the boundary layer mixing processes. The average ship position is shown by the + at 16 km for the ship track head with a standard deviation of 8 km. The spread of data points in Figure 5 is due to errors in relative wind and ship position calculations. Under the assumption that there is not significant bias in these errors, the average position should be a good estimate of the average ship position relative to ship track head. The time required for the effluent to mix through the boundary layer and increase cloud reflectance (observable in AVHRR imagery) can be estimated by dividing the separation distance by the relative wind speed. Applying this to each of the 99 cases results in an average time of 25 minutes with a standard deviation of 15 minutes.

2) Ship track width and dispersion

As turbulent processes broaden the ship plume, the resulting ship track broadens. Therefore observations of ship tracks in satellite imagery will lead to understanding of the turbulent conditions within the MABL. As a first approximation, the width of a track will depend on the mixing characteristics of the MABL and the time since emission of effluent from the ship.

The objective of this study is to combine ship tracks from different ships and times to examine the average characteristics. Since the ship and atmosphere are moving relative to one another, it is necessary to combine points along the track that are of the same age and not the same distance from the ship. The speed of movement away from a ship is determined by the wind and ship-motion vectors. The relative wind vector, given by the vector difference of the

ship-motion and wind vectors, describes the speed and direction that the effluent moves away from the ship. The time since emission of any fragment of the ship track is then calculated as the distance downtrack divided by the relative wind speed.

The relative wind vector points away from the ship and down the ship track. Given the same mixing environment, the effluent from a ship moving into the wind will move away from the ship faster than the effluent from a ship moving with the wind. In fact, if a ship is moving with the wind, the effluent will not move away from the ship except by turbulent mixing processes.

Figure 6 shows a set of ship tracks observed in the MAST operating area on 30 June 1994 at 0046 UTC. Two of the ships (A, B) are moving roughly into the wind and two of the ships (C, D) are moving roughly with the wind. The relative wind speed for ships A and B (into the wind) is 11.8 m s^{-1} and 23.4 m s^{-1} respectively. The relative wind speed for ships C and D (with the wind) is 5.2 m s^{-1} and 4.3 m s^{-1} respectively - a factor of two to six smaller than for the ships moving into the wind. Consequently, the width of ship tracks from ships A and B (into the wind) is 3.1 and 3.8 km respectively at 40 km downtrack, while from ships C and D (with the wind) the width is 10.5 and 6.1 km respectively at 40 km downtrack - a factor of 2-3 greater than the ships moving into the wind.

Pollution studies have historically modeled emissions from a continuous point source as a conical plume with a gaussian distribution across the plume (Turner, 1994). The environment conducive to ship track formation described above produces a boundary layer with near-neutral stability capped by a subsidence inversion aloft. Ship exhaust released in this type of marine boundary layer results in a trapped plume. When neutral atmospheric conditions exist, plumes are diffused by mechanical turbulence. The turbulence intensity is a function of sea surface roughness, height in the MABL, and, most importantly, wind speed.

There is currently no model describing long-range diffusion over water, especially not one that is based on actual field experiments extending over the ranges that ship tracks are observed. For this study we developed an estimation of the ship track horizontal plume dispersion parameter (σ_y = plume width) based on the opacity method introduced by Roberts (1923) and applied to dispersion studies by Gifford (1957, 1959, and 1980). The opacity method estimates σ_y directly from the observed brightness patterns of ship tracks. It relies on

observation of the maximum plume width and is independent on the source characteristics and cloud microphysics.

Figure 7 shows σ_y plotted versus track element age or time since emission. Time is calculated from the head point of ship tracks and therefore does not include separation time. This could add an average of 25 minutes to the age of each ship track. The dashed line is the Heffter (1965) equation ($d\sigma_y/dt = 1.853 \text{ km hr}^{-1}$) - used in long-range pollutant travel and dispersion predictions over land. The data after about one hour shows a similar slope to Heffter's equation but with significant scatter. The variability seen in Figure 7 is quite large and could be due to a combination of large-scale spatial variations in boundary layer properties such inversion height, stability, and ambient cloud reflectance. The findings reported here represent a data rich (>30,000 data points), statistically significant, characterization of long-range, over-water diffusion from a continuous point source and could be utilized to improve pollution transport and dispersion models.

c. Composite radiative characteristics

A single ship track displays a high degree of along-track variability in its radiative signature. The variability occurs predominantly on a scale of 1-25 km and is due to non-homogeneous stratus cloud, cirrus cloud interference, cloud roll structure, large-eddy size variations, and crossings with other ship tracks. The composite of many ship tracks will average out the variability in any single ship track, revealing the average ship track radiative and physical characteristics.

Figure 8 and 9 presents composite plots of relative track reflectance for AVHRR channel 1 and 3 (D1 and D3) which is the calculated fractional increase in LOW1 and LOW3 between the ambient cloud and the ship track values. The data set includes all 131 ship tracks (30,144 data points) from 52 different ships described above. The relative track reflectance is plotted verses age relative to the ship track head. The separation distance between ship and ship track (not known in all cases) is not included in the age calculation.

The trend line for D1 in Figure 8 has a value of 12% for relative track reflectance at zero age. This means that the near-head region of ship tracks are, on average, 12% more reflective of red-visible solar radiation than the ambient cloud in which it formed. Furthermore D1 has positive values out to about 5 hours of track age. This corresponds to an area of 1800 km^2

(assuming an average width of 9 km and relative wind speed of 40 km hr⁻¹) where the ship has generated more reflective cloud than in the ambient environment.

The strong signal for D3 seen in Figure 9 confirms that it is a better indicator of ship-induced effects on cloud microphysics than D1. The trend line steadily decreases from a zero-age value of 41.6%. On average the 3.7 μm radiation is being reflected 37% more by the ship track than the ambient cloud.

d. Ship effects on ship track characteristics

The ship to ship track correlation set contains 17 steam turbine ships and 114 diesel engine ships. Table 3 shows comparisons of ship track parameters for the two propulsion groups. Ship tracks from diesel ships are 18% longer, 32% older and 16% wider than ship tracks from steam turbine ships. While the neither ship type shows a significant difference between the ambient and track visible wavelength reflectance, diesel ship tracks are 27% brighter than the ambient cloud in the near-infrared compared to steam ship tracks that are only 7% brighter than the background cloud. These observations are consistent with diesel ships producing greater numbers of CCN that are able to perturb cloud droplet size (Hobbs et al., this issue). More CCN would suggest a longer time required for the plume to disperse horizontally to the point where concentrations were reduced to background values. In addition, more aerosol particles would suggest a greater impact on cloud droplet size and therefore greater influence on cloud reflectance, especially at 3.7μm wavelength.

A ship's power rating has a measurable impact on the radiative and physical characteristics of the ship track it produces. Table 4 shows ship track characteristics for equal size subsets by power rating: > 23,500 kW and < 13,000 kW. Ships with high total designed shaft power ratings produce ship tracks that are 20% longer, 10% older, and 8% wider than ships with low power ratings. Similar to comparisons by propulsion type, while very little difference is seen for visible wavelength cloud reflectance, high powered ships produce a greater increase in cloud reflectance at the near-infrared wavelength than low powered ships. These results are consistent with the fact that higher power ships produce more aerosols (Hobbs et al., this issue). The aerosol and CCN concentration is therefore higher in the cloud, which results in greater persistence of the perturbation to droplet size and cloud brightness.

4. Composite ship track properties

Figure 10 illustrates composite ship track characteristics of important environmental, radiative, and physical parameters determined in this study. Figure 10 also lists some important summary statistics. The composite ship track is $296(\pm 233)$ km long and averages $9(\pm 5)$ km wide. The average age of the oldest part of the composite ship track is $7.3(\pm 6)$ hours old while many tracks are older than 12 hours. The ship is, on the average $16(\pm 8)$ km from the head of the ship track along the relative wind vector. This separation distance corresponds to a time of $25(\pm 15)$ minutes required to transport the ship effluent through the marine boundary layer and perturb the cloud microphysics.

The set of ship tracks examined in this study formed in marine boundary layers that were between 300 and 750 m deep, and no tracks formed in boundary layers above 800 m. The tracks form in high relative humidity, small air-sea temperature differences, and moderate winds (average of $7.7(\pm 3.1)$ m s⁻¹). The ambient cloud reflectance in AVHRR channel 3 is $11(\pm 4)\%$ while the composite ship track value is $14(\pm 5)\%$. The relative track brightness is $7(\pm 26)\%$ and $37(\pm 34)\%$ for visible and near-infrared wavelengths respectively.

Ships that produce more aerosol - such as diesel relative to steam turbines, and ships with high power rating - on the average produce ship tracks that are brighter (especially at near-infrared wavelengths), wider and longer lived than ships that produce less aerosol. This result directly supports MAST Hypothesis 1.1a that states that aerosol from the ship's stack are responsible for the formation of ship tracks (Durkee et al., this issue). In addition, the time to transport ship effluent from stack to cloud (20-25 minutes) is not shorter than expected due to natural turbulent processes in the marine boundary layer. Therefore, the heat or momentum inputs from the ship are not significantly enhancing the transport of ship effluent through the marine boundary layer.

Finally, this paper presents initial results of the analysis of dispersion properties of marine boundary layers from studies of ship tracks. The results shown here indicate that dispersion processes are highly variable with probable dependence on wind speed, stability, boundary layer depth, and the orientation of the ship's course relative to the wind. As ship track to ship correlations increase, the data set should become large enough to begin to address these dependencies.

Acknowledgments. The US Air Force managed Space Test Program provided operational support for space shuttle photography of ship tracks. Special thanks goes to CAPT John Hennesy, CAPT David Goldstein, CAPT Jeff Long and Mr. Ralph Hull. MAST was principally funded by the Office of Naval Research Accelerated Research Initiative called the Surface Ship Cloud Effects Project.

REFERENCES

- Albrecht, B.A., 1989: Aerosols, cloud microphysics and fractional cloudiness. *Science*, **245**, 1227-1230.
- Bowley, C. J., 1967: Comments on atmospheric requirements for the genesis of anomalous cloud lines. *J. Atmos. Sci.*, **24**, 569-597.
- Brenner, J., 1994: Continental aerosol effects on stratocumulus microphysics during MAST 1994. M.S. Thesis, Naval Postgraduate School, Monterey, CA, 60pp.
- Bretherton, C.S., M.C. Wyant, I.M. Brooks, and T.J. Garrett, 1996: Ship tracks and marine boundary layer decoupling, *J. Atmos. Sci.*, submitted.
- Charlson, R.J., J.E. Lovelock, M.O. Andreae, and S.G. Warren, 1987: Oceanic phytoplankton, atmospheric sulphur, cloud albedo, and climate. *Nature*, **326**, 655-661.
- Charlson, R.J., S.E. Schwartz, J.M. Hales, R.D. Cess, J.A. Coakley Jr., J.E. Hansen and D.J. Hofman, 1992: Climate forcing by anthropogenic aerosols. *Science*, **255**, 423-430.
- Coakley, J.A. Jr., R.L. Bernstein and P.A. Durkee, 1987: Effect of ship-stack effluents on cloud reflectivity. *Science*, **237**, 1020-1022.

Coakley, J.A., P.A. Durkee, K. Nielsen, J.P. Taylor, S. Platnick, B.A. Albrecht, D. Babb, F.-L.

Chang, W.R. Tahnk, C.S. Bretherton, and P.V. Hobbss, 1996: The appearance and disappearance of ship tracks on large spatial scales, *J. Atmos. Sci.*, submitted.

Conover, J.H., 1966: Anomalous Cloud Lines. *J. Atmos. Sci.*, **23**, 778-785.

Durkee, P.A., K. J. Noone, R. T. Bluth, 1996: The Monterey Area Ship Track (MAST) Experiment. *J. Atmos. Sci.*, submitted.

Gifford, F.A., 1957: Relative atmospheric diffusion of smoke puffs, *J. Met.* **14**, 410-414.

Gifford F.A., 1959: Smoke plumes as quantitative air pollution indices. *Int. J. Air Pollut.* **2**, 42-50.

Gifford, F.A., 1980: Smoke as a Quantitative Atmospheric Diffusion Tracer, *Atmos. Environ.* **14**, 1119-1121.

Heffter, J.L. , 1965: The variation of horizontal diffusion parameters with time for travel periods of one hour or longer. *J. Appl. Meteor.*, **4**, 153-156.

Hobbs, P.V., T.J. Garrett, R.J. Ferek, S.R. Strader, D.a. Hegg, G.M. Frick, W.A. Hoppel, R.F. Gasparovic, L.M. Russell, D.W. Johnson, C. O'Dowd, P.A. Durkee , K.E. Nielsen, and G. Innis, 1996: Emissions from ships with respect to their effects on clouds. *J. Atmos. Sci.*, submitted.

Kirschbaum, A. R., 1994: The design and implementation of the Military Applications of Shiptracks Experiment on STS-65. M.S. Thesis, Naval Postgraduate School, Monterey, CA, 54pp.

- Mineart, G.M., 1988: Multispectral satellite analysis of marine stratocumulus cloud microphysics. M.S. Thesis, Naval Postgraduate School, Monterey, CA, 138pp.
- Porch, W. M., C.-Y. Kao, M. I. Buckwald, W. P. Unruh, P. A. Durkee, E. E. Hindman, J. G. Hudson, 1995: The effects of external forcing on the marine boundary layer: Ship trails and a solar eclipse. *The Global Atmosphere and Ocean System*, **3**, 323-340.
- Roberts, O.F.T., 1923: The theoretical scattering of smoke in a turbulent atmosphere. *Proc. Roy. Soc.* **A104**, 640-654.
- Skupniewicz, C.E., and Schacher, G.E., 1986: Parameterization of plume dispersion over water. *Atmos. Environ.*, **7**, 1333-1340.
- Turner, D.B., 1994: *Workbook of Atmospheric Dispersion Estimates, an Introduction to Dispersion Modeling*. CRC Press, Inc., Boca Raton, FL.

TABLES

Table 1. Composite environmental conditions in ship track and non-ship track regions.

Environmental Parameter	Ship track minimum/ mean / maximum (standard deviation)	Non-Ship track minimum/ mean / maximum (standard deviation)
Boundary Layer Depth (m)	200/ 504 /716 (125)	180/ 812 /1346 (316)
Air Temperature (C)	11.2/ 14.6 /19.9 (1.9)	12.3/ 16.5 /19.9 (2.4)
Sea Surface Temperature	11.0/ 14.9 /19.0 (1.7)	13.4/ 16.8 /19.5 (1.4)
Air -Sea Temperature Difference	-2.4/ -0.3 /1.8 (0.8)	-0.9/ 0.2 /1.3 (0.7)
Surface Pressure (mb)	1014.3/ 1018.3 /1022.0 (2.4)	1014.4/ 1017.4 /1022.8 (2.2)
Relative Humidity (%)	72/ 90 /99 (6.5)	62/ 82 /99 (10.8)
Cloud thickness (% MABL depth)	20/ 47 /88 (19)	9/ 41 /70 (19)
Wind Speed (m s ⁻¹)	0.3/ 7.8 /12.3 (3.0)	0.9/ 5.5 /11.7 (3.5)

Table 2. Summary of Correlation Statistics for MAST. The value in parenthesis is the number used for this study.

Propulsion Type	No. of different ships	No. of correlations
Steam Turbine	13 (8)	33 (17)
Diesel Engine	61 (44)	176 (114)
Totals	74 (52)	209 (131)

Table 3. Comparison of ship track parameters for diesel and steam ships. The difference of all means are significant at the 95% level except for the LOW1 values.

Variable	Diesel	Steam
Length (km)	301.6	254.6
Age (hr)	7.5	5.7
Width (km)	9.32	8.00
Ambient LOW1 (%)	36.4	32.9
Track LOW1 (%)	36.2	33.0
Ambient LOW3 (%)	11.1	10.5
Track LOW3 (%)	14.1	11.2

Table 4. Comparison of ship track parameters for all ships with power rating >23,500 kW and <13,000 kW. The mean differences are significant at the 95% level except for the LOW1 values.

Variable	>23,500 kW	< 13,000 kW
Length (km)	314	263
Age (hr)	7.3	6.6
Width (km)	9.8	9.0
Ambient LOW1 (%)	38.9	33.1
Track LOW1 (%)	39.2	33.1
Ambient LOW3 (%)	10.9	10.9
Track LOW3 (%)	14.1	13.7

FIGURES

Figure 1. A histogram over boundary layer height of conducive and non-conductive cases from the analysis of the SEAHUNT and MAST data sets. The solid line is the average number of ship tracks observed per case as a function of boundary layer height.

Figure 2. The geographical location of the 1362 ship track heads identified in AVHRR imagery during the MAST experiment. The head of the track is denoted by a dot.

Figure 3. Photograph taken by shuttle astronauts during mission STS-65 off the west coast of Chile on 20 July 1994.

Figure 4. A visible image from the RC-10 camera aboard the NASA ER-2 aircraft taken at 1840 UTC on 13 June 1994.

Figure 5. A plot of the calculated ship position for the 99 correlations relative to the ship track head observed in AVHRR data. The + indicates the average ship position.

Figure 6. Ship tracks observed in AVHRR channel 3 within the MAST operating area on 30 June 1994 at 0046 UTC. The wind and ship motion vectors are shown with arrows.

Figure 7. A plot of σ_y versus track element age or time since emission. Dashed line is the curve derived by Heffter (1965).

Figure 8. Composite relative track reflectance for AVHRR channel 1 (0.63 μm wavelength) against track age.

Figure 9. Composite relative track reflectance for AVHRR channel 3 (3.7 μm wavelength) against track age.

Figure 10. Composite ship track characteristics of important environmental, radiative, and physical parameters determined in this study.

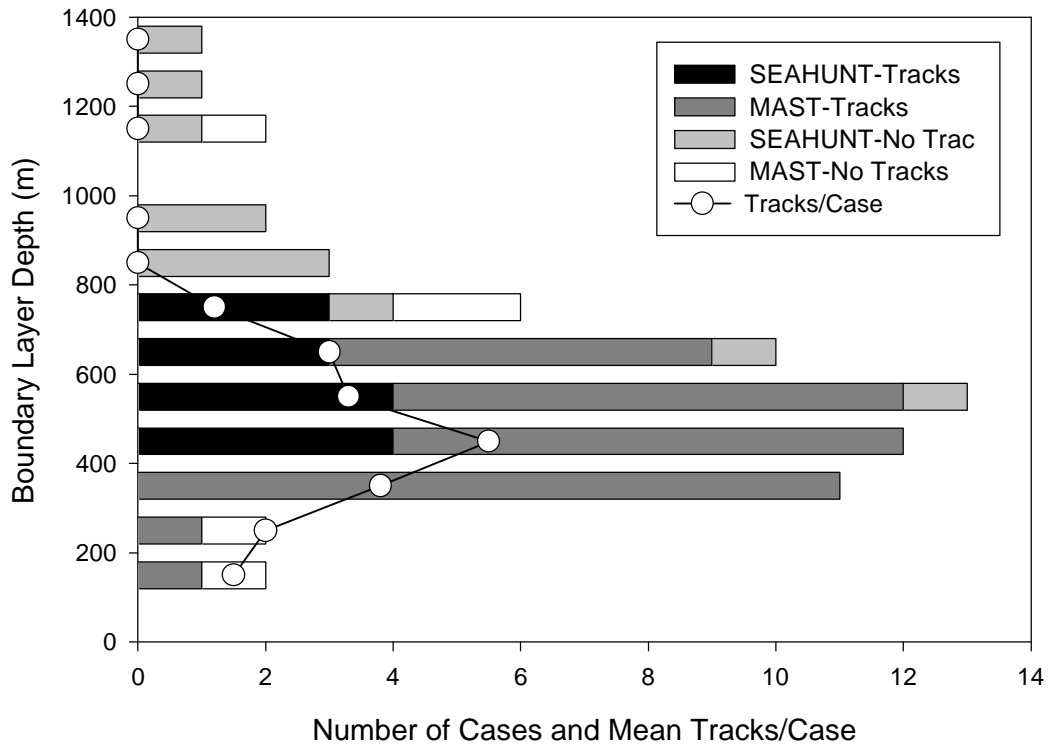


Figure 1. A histogram over boundary layer height of conducive and non-conductive cases from the analysis of the SEAHUNT and MAST data sets. The solid line is the average number of ship tracks observed per case as a function of boundary layer height.

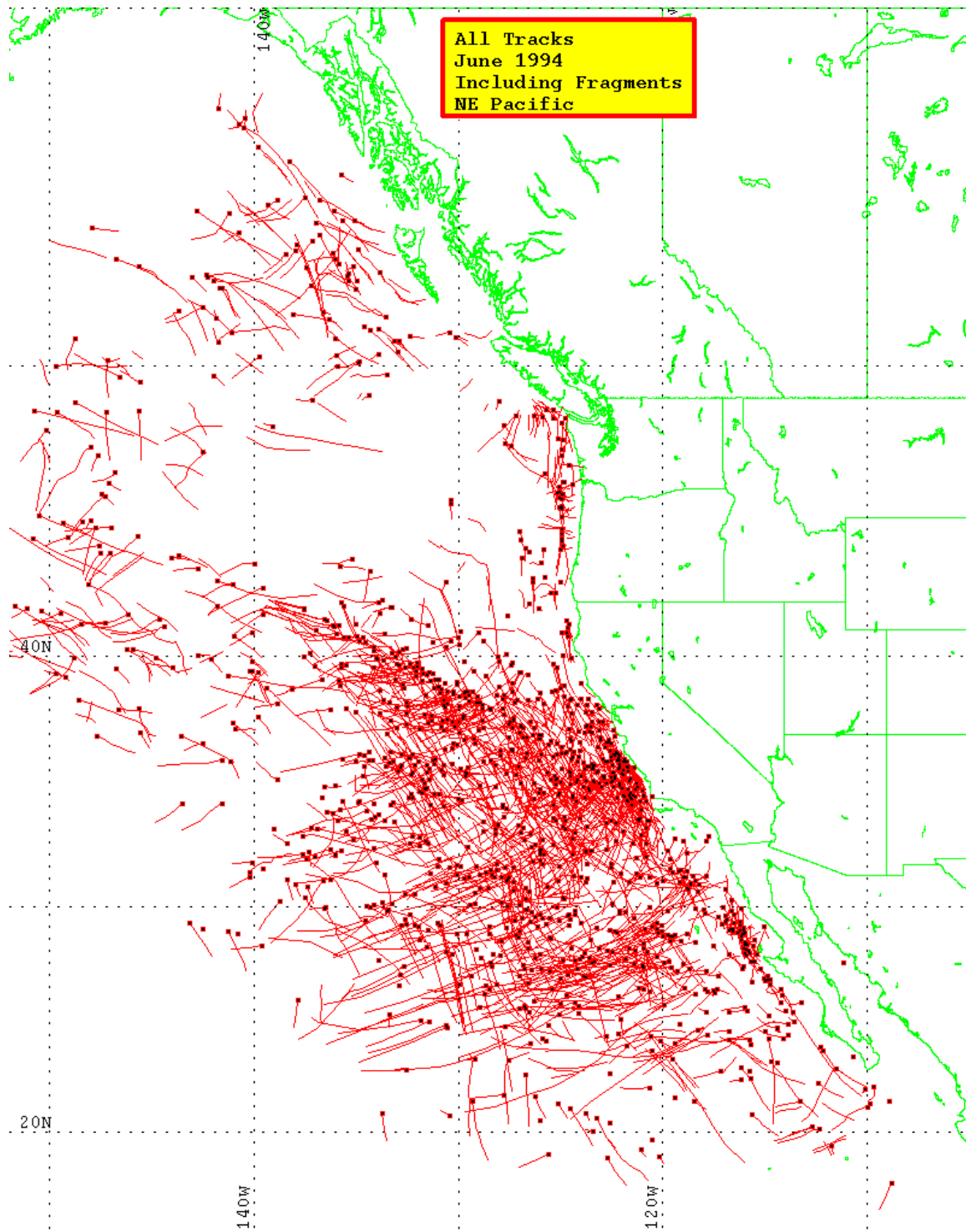


Figure 2. The geographical location of the 1362 ship track heads identified in AVHRR imagery during the MAST experiment. The head of the track is denoted by a dot.



Figure 3. Photograph taken by shuttle astronauts during mission STS-65 off the west coast of Chile on 20 July 1994.

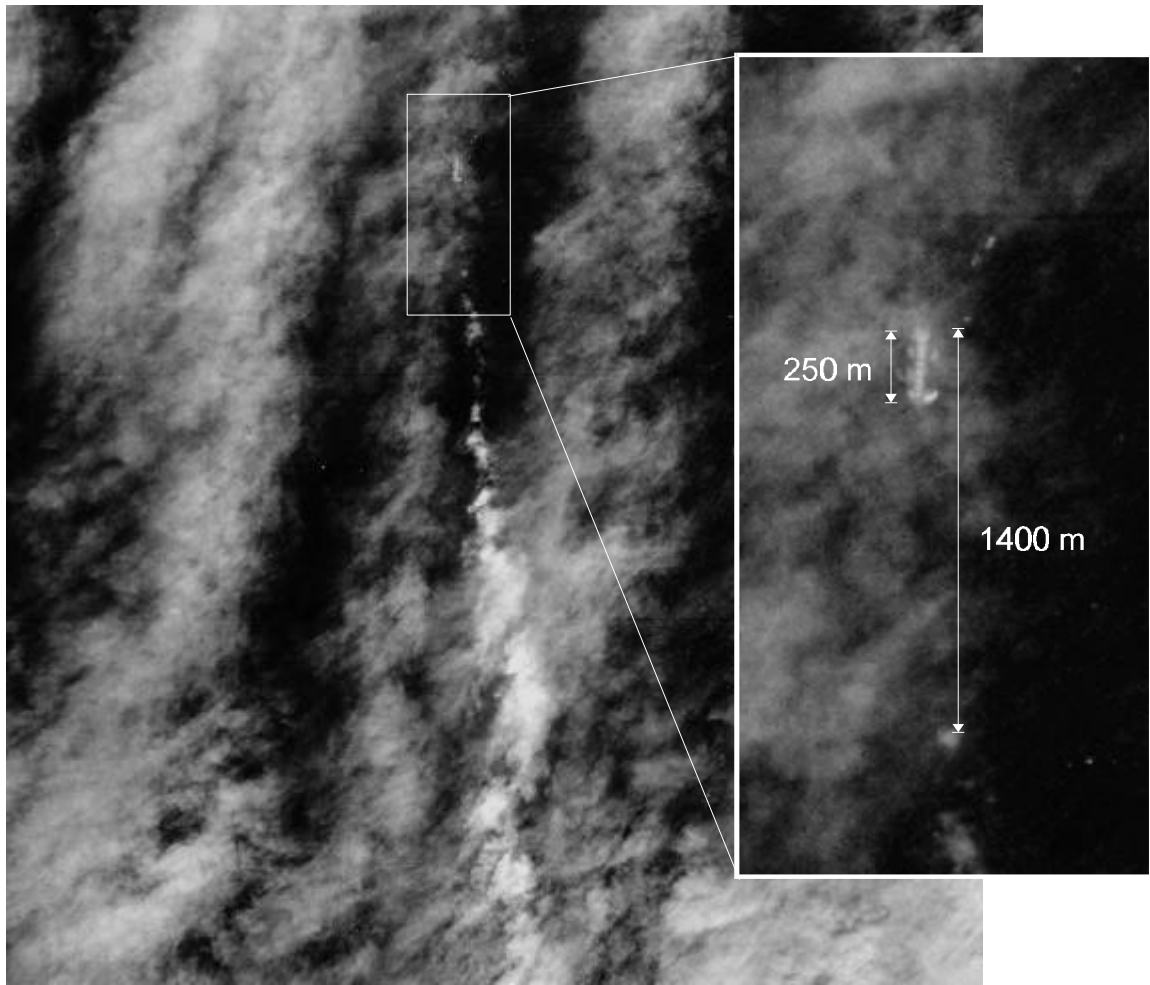


Figure 4. A visible image from the RC10 camera aboard the NASA ER-2 aircraft taken at 1840 UTC on 13 June 1994.

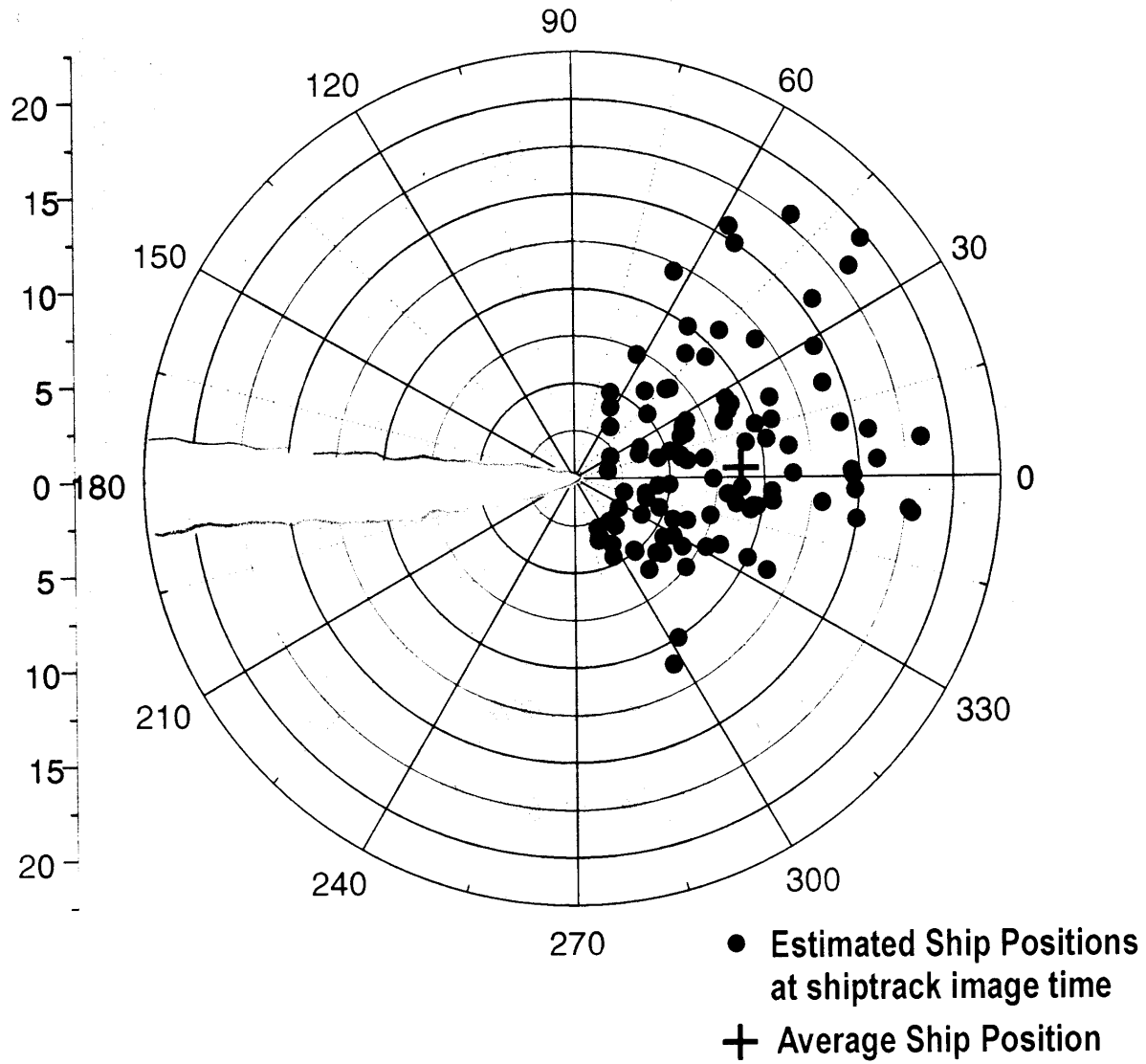


Figure 5. A plot of the calculated ship position for the 99 correlations relative to the ship track head observed in AVHRR data. The + indicates the average ship position.

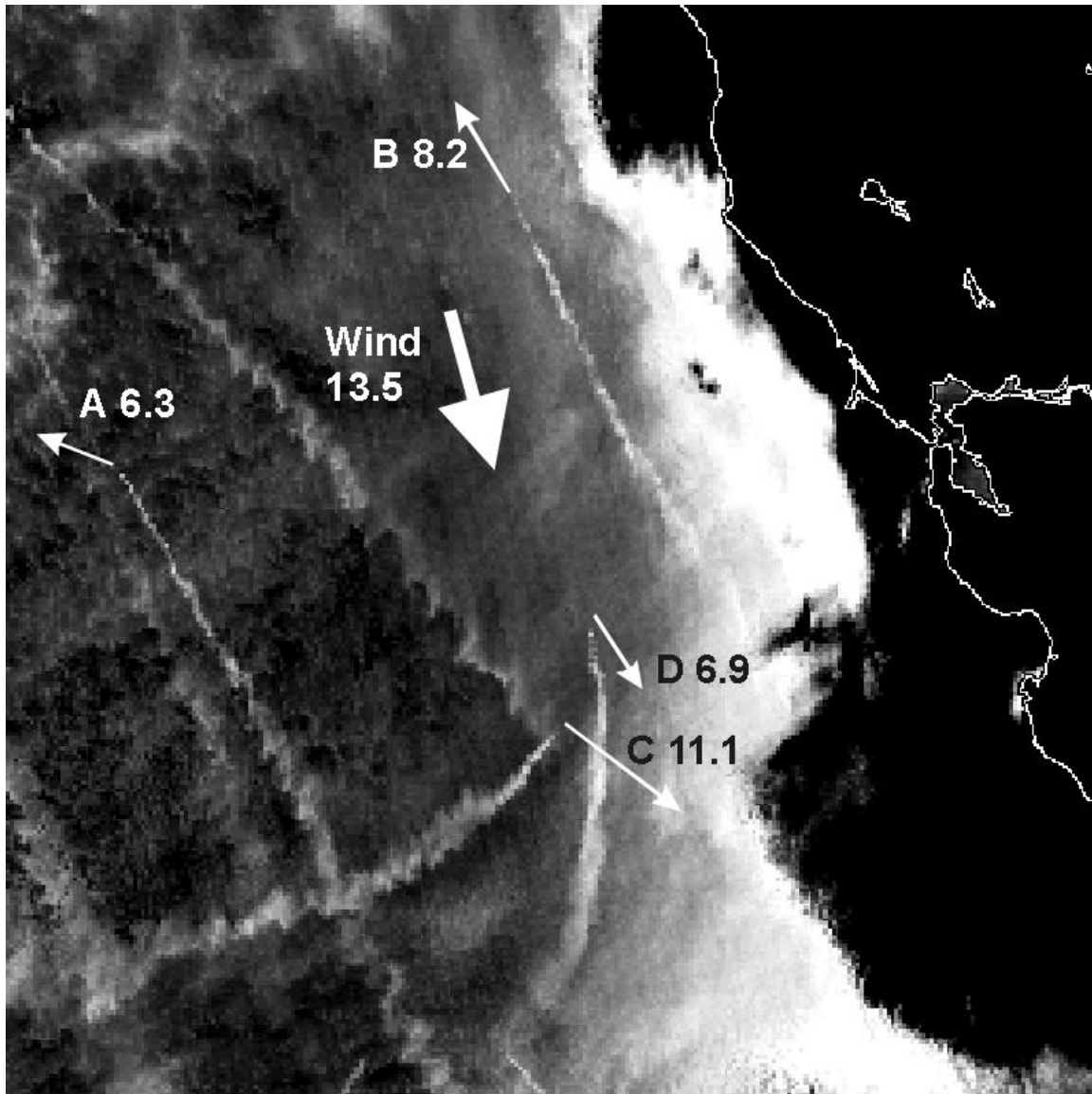


Figure 6. Ship tracks observed in AVHRR channel 3 within the MAST operating area on 30 June 1994 at 0046 UTC. The wind and ship motion vectors are shown with arrows.

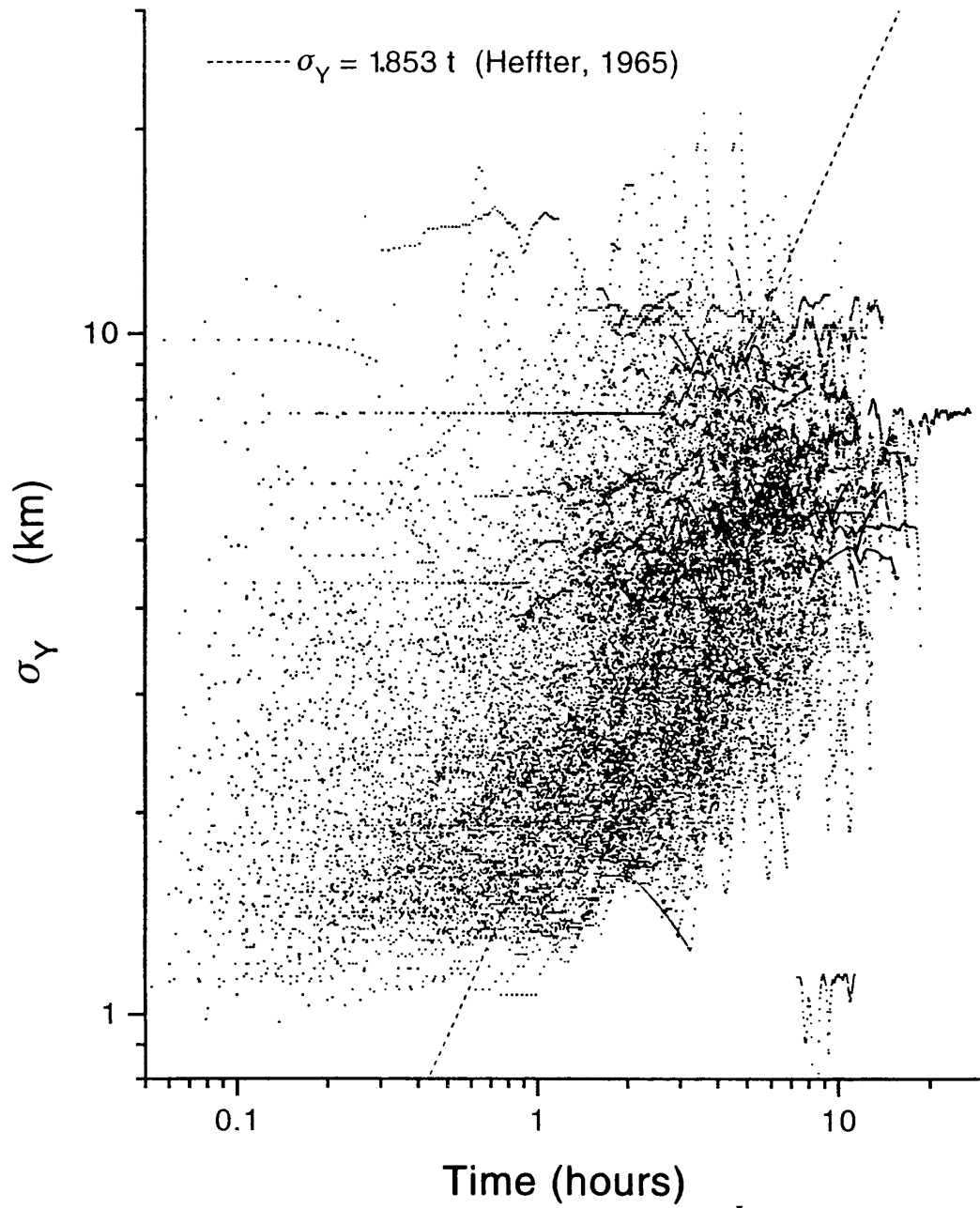


Figure 7. A plot of σ_y verses track element age or time since emission.

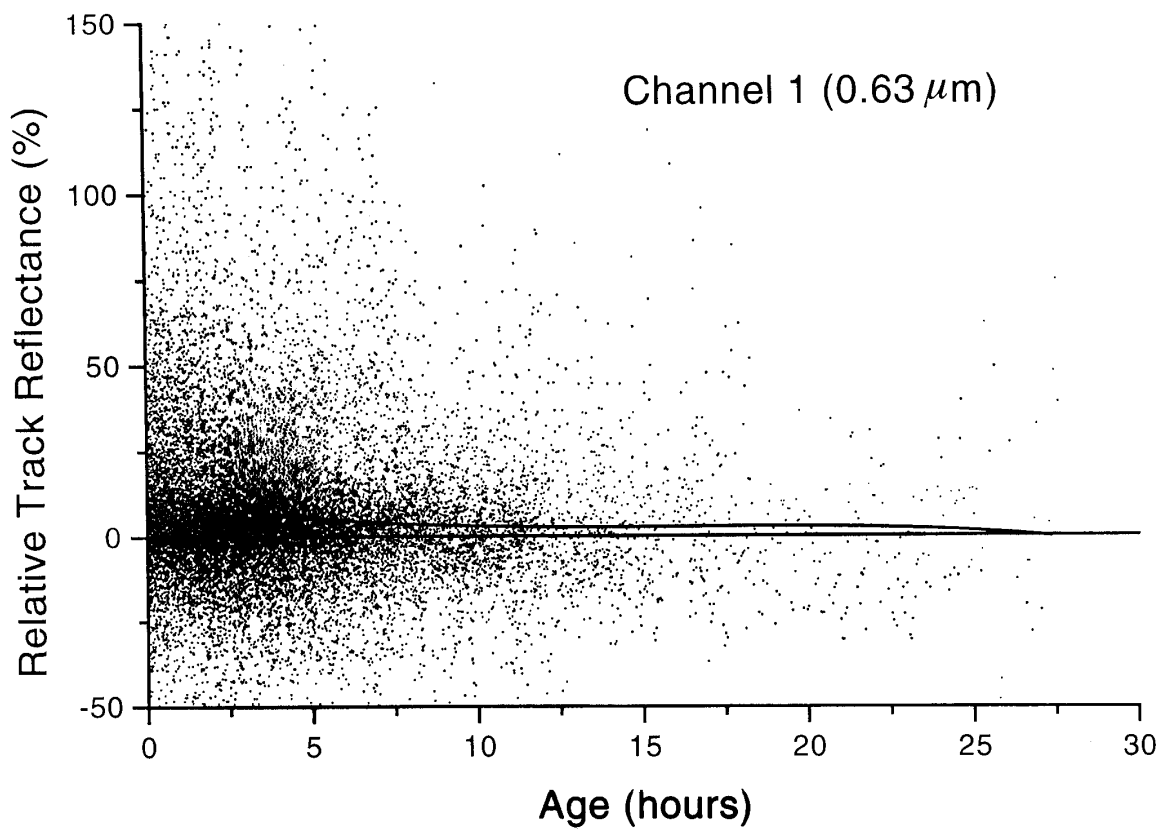


Figure 8. Composite relative track reflectance for AVHRR channel 1 (0.63 μm wavelength) against track age.

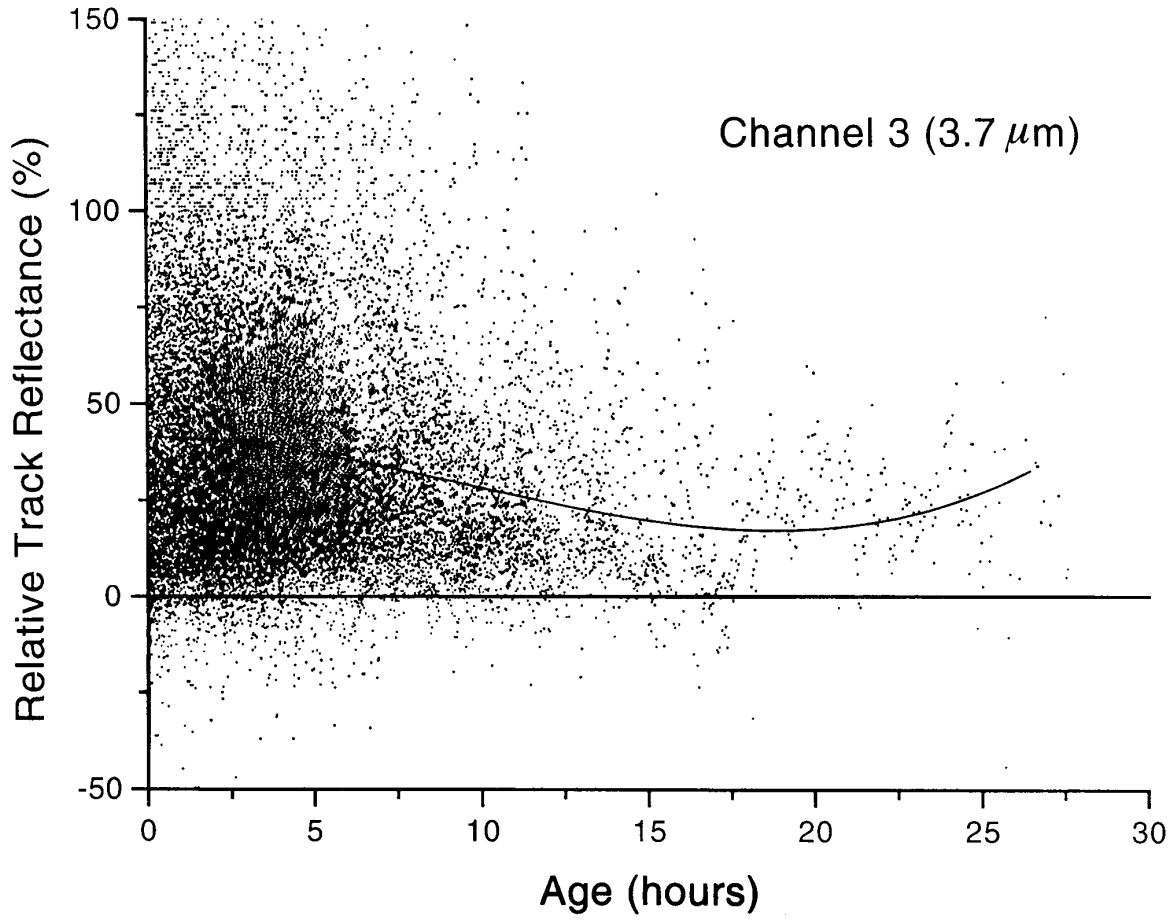


Figure 9. Composite relative track reflectance for AVHRR channel 3 (3.7 μm wavelength) against track age.

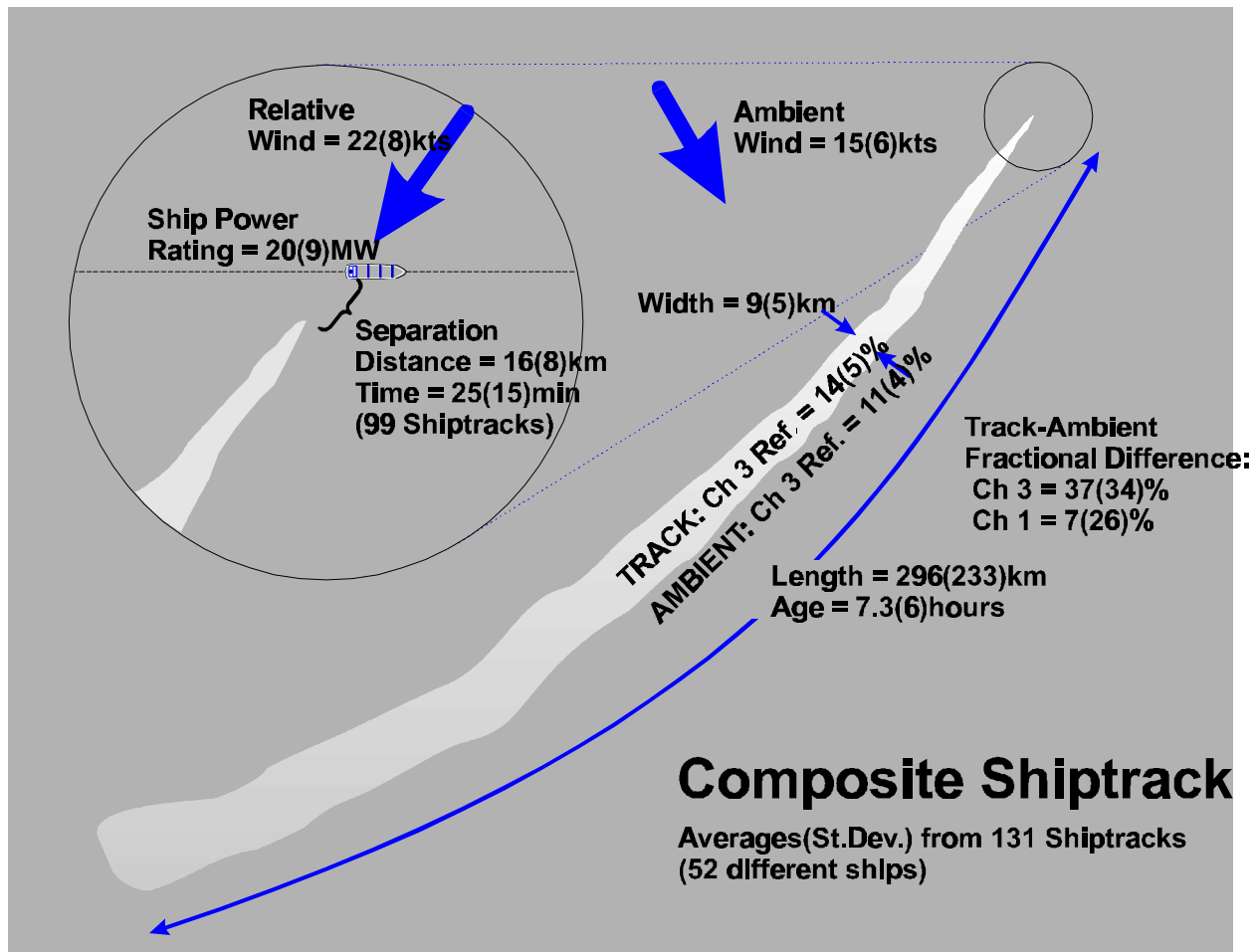


Figure 10. Composite ship track characteristics of important environmental, radiative, and physical parameters determined in this study.